RESEARCH ARTICLE

Response of surface ozone concentration to emission reduction and meteorology during the COVID-19 lockdown in Europe

Adrien Deroubaix[1] | Guy Brasseur[1,2] | Benjamin Gaubert[2] | Inga Labuhn[3] | Laurent Menut[4] | Guillaume Siour[5] | Paolo Tuccella[6]

[1]Max Planck Institute for Meteorology, Hamburg, Germany

[2]Atmospheric Chemistry Observations & Modeling Laboratory (ACOM), National Center for Atmospheric Research, Boulder, CO, USA

[3]University of Bremen, Institute of Geography, Bremen, Germany

[4]LMD/IPSL, Ecole Polytechnique, Université Paris Saclay, ENS, IPSL Research University; Sorbonne Université, CNRS, Palaiseau, France

[5]Laboratoire Interuniversitaire des Systèmes Atmosphériques (LISA), UMR CNRS 7583, Université Paris Est Créteil et Université de Paris, Institut Pierre Simon Laplace, Créteil, France

[6]Departement of Physical and Chemical Sciences, University of L'Aquila, L'Aquila, Italy

Correspondence
Adrien Deroubaix, Max Planck Institute for Meteorology, Hamburg, Germany.
Email: adrien.deroubaix@mpimet.mpg.de

Funding information
Max-Planck-Gesellschaft

Abstract

The lockdown period (March–May 2020) during the COVID-19 pandemic in Europe led to a reduction in the anthropogenic emissions of primary pollutants. For three-quarters of over 1,100 available monitoring stations, the average nitrogen dioxide (NO_2) concentrations decreased by at least 2.7 $\mu g \cdot m^{-3}$ (or 25%) compared with the average concentrations recorded during the same period of the previous seven years. This reduction was not specific to urban or rural areas because the relative reduction was of similar magnitude in both areas. The ozone (O_3) response differed spatially, with positive anomalies in Northern Europe and negative anomalies in Southwestern Europe. Reduced cloudiness and related enhanced radiation in Northern Europe played a significant role in the increase of surface O_3 concentrations by shifting the photochemical partitioning between NO_2 and O_3 toward more O_3. The level of total oxidant ($O_x = O_3 + NO_2$) remained unchanged, except in Southwestern Europe where it decreased. Several episodes lasting a few days of a high level of total oxidants were observed in Northern Europe. The results illustrate the complexity of the atmospheric response to the unprecedented reduction in the emission of primary pollutants.

KEYWORDS

air quality, COVID-19, Europe, ozone, sensor networks, topo-climate, urban

1 | INTRODUCTION

COVID-19 lockdown restrictions were imposed worldwide in early 2020, first in China, starting in January 2020, and then in early and mid-March across Europe. In mid-May, restrictions started to be gradually lifted in Europe. Consequently, anthropogenic emissions, especially those related to traffic, were substantially reduced first in China (Le *et al.*, 2020; Shi and Brasseur, 2020) and later elsewhere. The concentration of nitrogen dioxide (NO_2) observed at monitoring stations decreased by up to 60%, whereas a simultaneous increase in ozone (O_3) concentration by a factor 1.5–2 was reported (Shi and Brasseur, 2020). Moreover, unexpected increases of sulfur dioxide (SO_2) were

monitored during the lockdown period in some regions of China (e.g. the region of Hangzhou), probably due to higher coal consumption for heating (Wang *et al.*, 2020).

Substantial changes in NO_2 columns measured by the spaceborne TROPOMI instrument have been reported at locations with heavy lockdown measures due to the COVID-19 pandemic. In many Chinese cities, NO_2 column densities decreased by at least 40% (Bauwens *et al.*, 2020). In North American and European cities, a decrease of up to 40% was observed (Bauwens *et al.*, 2020). In Spain, for example, the average reduction of NO_2 during the lockdown compared with a "business-as-usual" emission scenario was estimated to be close to 40% using machine learning fed by meteorological data (Petetin *et al.*, 2020).

Disentangling the lockdown effects on NO_2 from the natural variability induced by meteorological conditions is essential to build accurate emissions for air quality modeling (Goldberg *et al.*, 2020). Further, short-term perturbations of NO_2 must be put in the context of the long-term trends of pollutant concentrations. Over the two last decades, NO_2 trends have been negative in Europe, while O_3 concentrations remained high (Colette *et al.*, 2015; Yan *et al.*, 2019).

Ordóñez *et al.* (2020) showed that the O_3 concentration increased in Europe during the lockdown, except in the Iberian Peninsula and in southwestern areas of France. Using general additive models at each monitoring station to attribute the changes in surface O_3 concentrations, they conclude that the meteorological variability outweighed the effects of emission reductions in both urban and rural areas.

The numerous links between O_3 formation and meteorology, involving several processes, raise questions about the meteorological influence on the oxidation capacity of the low troposphere, especially in urban areas where NO_2 reductions were largest (Kroll *et al.*, 2020). Moreover, based on a modelling study, Menut *et al.* (2020) demonstrated that the O_3 perturbation during the lockdown period was different in urban areas throughout Western Europe due to nonlinear chemical effects. This is further highlighted by Sicard *et al.* (2020) who showed a variable O_3 increase in four Southern European cities (Nice in France, Rome and Turin in Italy, and Valencia in Spain), ranging from 2.4% in Valencia to 27% in Turin compared with the period 2017–2019. The purpose of the present study is to understand the causes of the surface O_3 concentration change in response to the exceptional short-term reduction of anthropogenic emissions during the COVID-19 lockdown period in Europe. Anomalies are characterized in the concentrations of five regulated pollutants: carbon monoxide (CO), NO_2, SO_2, O_3 and particulate matter (PM_{10}) in rural and urban environments (compared with the previous seven years) associated with anomalies of different meteorological variables. This allows the investigation of the possible causes of the observed O_3 concentration changes, which could be related to the changes in primary pollutant emissions, but also to concomitant changes in meteorology and photochemistry. The study will further focus on the evolution of the total oxidant concentrations (also called odd oxygen), that is, $O_x \approx O_3 + NO_2$ (Wang and Jacob, 1998).

The study is based on measurements made at surface monitoring stations together with modelled meteorological conditions. Air quality data and other data sources are referred to in Section 2. Section 3 presents the distribution of the concentration changes, and Section 4 their spatial patterns. The O_3 response is analysed in Section 5, and its consequences on the total oxidant level in Section 6. A discussion and perspectives are given in Section 7.

2 | DATA AND METHODS

Air quality, meteorological conditions and population density data were obtained for the spatial domain under consideration that extends from 11° W to 19° E and from 35° to 60° N. The focus here is on the period March 18–May 18 of 2013–2020.

Measured concentrations of regulated pollutants from national monitoring networks were retrieved from the European Air Quality e-Reporting database (AirBase), which provides near-real-time air-quality data for Europe in a standardized format (AQ e-Reporting, 2020). The data available are hourly concentrations in the case of CO, NO_2, SO_2 and O_3, and daily concentrations in the case of PM_{10}. The domain includes 1,680 AirBase stations. However, data from 1,308 stations were used the present study as stations were only selected with at least 70% of days of the period March 18–May 18 (for each year) filled with at least one hourly value for the respective pollutant.

Meteorological variables were obtained from the European Centre for Medium-Range Weather Forecasts' (ECMWF) Copernicus Atmosphere Monitoring Service (CAMS) global forecast at a horizontal resolution of approximately 40 km (T511 spectral) on 137 vertical levels from the surface up to 0.1 hPa. Through the CAMS global archived analysis and forecast daily data, 6 hr analyses of the following meteorological variables were downloaded (Inness *et al.*, 2019): 2 m temperature, 2 m dew point, mean sea level pressure, potential vorticity at 300 hPa, 10 m zonal wind, 10 m meridional wind, total cloud cover and downward surface solar radiation (forecast accumulated over 24 hr). The 2 m relative humidity

field was calculated on the basis of the temperature and dew point fields. The 10 m wind speed field was calculated from the zonal and meridional wind fields. The potential vorticity at 300 hPa was selected as a proxy for the downward stratospheric transport (e.g. Doche *et al.*, 2014).

Population density data were taken from the Gridded Population of the World Version 3 (GPWv3) data set, which has a spatial resolution of 1×1 km (CIESIN/CIAT, 2005; it is presented over the studied domain in Figure S1 in Appendix S1 in the additional supporting information). "Urban" and "rural" station types were defined based on the European Union's "high-density areas" threshold of 1,500 inhabitants·km^2. This leads to 485 "urban" stations (above this threshold) and 1,195 "rural" stations (below this threshold). With this methodology, urban sites are clearly located in areas with high anthropogenic emissions, whereas rural sites include a large diversity of environments.

Temporal anomalies were analysed by comparing the atmospheric quantities for the period March 18–May 18, 2020 (i.e. the lockdown period) with the same quantities for the previous seven years (2013–2019). For pollutants, two metrics were used to characterize the chemical environment at each station location using hourly measurements: (1) mean concentrations; and (2) the median of the hourly daily maximum concentrations. Anomalies are expressed as absolute and relative differences between 2020 and the 2013–2019 average.

3 | CHANGES IN THE CONCENTRATIONS OF REGULATED POLLUTANTS

At each station, the mean concentrations of regulated pollutants during the lockdown period were compared with the mean concentrations of the same pollutants averaged over the previous seven years. The distribution of absolute and relative differences (i.e. anomalies) given by five percentiles (10th, 25th, 50th, 75th, 90th) are presented for all stations (Table 1) and with a distinction between urban and rural stations (see Tables S1 and S2 in Appendix S1 in the additional supporting information).

Note the clear reduction in the average concentrations of NO_2, for which even the 90th percentile of the anomalies is negative (Table 1). Thus, at least 90% of the stations (P10) have monitored a reduction in NO_2 concentrations of at least 1 μg·m^{-3}, or 14%. In the case of O_3, the median (P50) of the anomalies is positive (4.3 μg·m^{-3}, or 7%), which means that a majority of the available stations have reported an increase in the average concentration. For PM_{10}, the median (50th percentile) of the anomalies is slightly negative (−0.7 μg·m^{-3}, or −4%), and the 75th percentile (P75) is positive (1.6 μg·m^{-3}, or −6%). Note that on March 28, a severe dust event over Southeast Europe led to strong positive PM_{10} anomalies for three days (Menut *et al.*, 2020).

The present authors' confidence in the database to represent accurately the distribution of the concentration anomalies across Europe is high for NO_2 and O_3 because 71% and 68% of the stations provide data (i.e. 1,196 and 1,148 stations, respectively), and to a lesser extent for PM_{10} with 53% (i.e. 895 stations).

For CO and SO_2, the number of monitoring stations is low (12% and 27%). Nevertheless, it can be observed that the median of the anomalies is −13.5 μg·m^{-3} (−5%) for CO and −0.2 μg·m^{-3} (−11%) for SO_2. Note that the 75th and 90th percentiles of CO and SO_2 are positive (Table 1), which shows that, in some regions, NO_2 decreased while CO and SO_2 increased. This suggests that traffic decreased while other emission sources such as residential or industrial emissions increased.

It can be expected that the strongest reduction in concentrations of primary pollutants happen in areas where human activities are the most intense. In other words, the reduction may be stronger at urban stations than at

TABLE 1 Anomalies of the mean concentrations of carbon monoxide (CO), nitrogen dioxide (NO_2), sulfur dioxide (SO_2), ozone (O_3) and particulate matter (PM_{10}) in 2020 compared with the average of the previous seven years (2013–2019) for the period March 18–May 18, 2020, measured at 1,308 European Air Quality e-Reporting database (AirBase) stations

	P10		P25		P50		P75		P90		
	μg·m^{-3}	%	μg·m^{-3}	%	μg·m^{-3}	%	μg·m^{-3}	%	μg·m^{-3}	%	% availability
CO	−131.2	−35%	−50.5	−18%	−13.7	−5%	30.8	13%	154.6	49%	12%
PM_{10}	−4.2	−22%	−2.6	−14%	−0.7	−4%	1.0	6%	3.0	16%	53%
NO_2	−12.1	−59%	−8.5	−50%	−5.2	−37%	−2.7	−25%	−1.0	−14%	71%
O_3	−9.7	−13%	−2.6	−4%	4.3	7%	8.5	14%	11.7	20%	68%
SO_2	−1.9	−55%	−0.9	−35%	−0.2	−11%	0.2	15%	1.1	60%	27%

Note: The distribution of the anomalies for all stations is given by five percentiles (P10, P25, P50, P75, P90); "% availability" indicates the percentage of available stations. Anomalies are presented in terms of concentrations (μg·m^{-3}) and of relative change (%) against the seven year average.

rural stations. To test this hypothesis, the same analysis is performed separately for urban and rural stations (as defined in Section 2) to investigate the pollutant concentration changes depending on population density.

The analysis reveals that the relative concentration changes are very similar for urban and rural stations (see Tables S1 and S2 in Appendix S1 in the additional supporting information). As expected, the NO_2 absolute anomalies are highest for urban stations (-7.9 µg·m^{-3}) compared with rural stations (-3.9 µg·m^{-3}), but the relative changes are similar for both types of stations (-40% for urban and -35% for rural stations). This result suggests that the mobility restrictions have led to comparable relative reductions of NO_2 emissions in urban and rural areas.

The O_3 absolute anomalies show an increase for both urban (6.8 µg·m^{-3}) and rural stations (3.1 µg·m^{-3}), although the relative anomalies show a comparable increase for those two areas (11% in urban stations and 5% in rural stations). This result clearly suggests that areas with stronger reduction in NO_2 concentrations led to higher increase in O_3 concentrations. It is concluded that a clear reduction of the NO_2 concentration averages

was monitored during the lockdown period, but this is not the case for O_3 and PM_{10} concentrations.

4 | SPATIAL PATTERNS OF NO_2 AND O_3

Although the analysis shows that there are distinct pictures for NO_2 and O_3 concentrations during the lockdown period, it was investigated whether there were spatial discrepancies for NO_2, O_3 and PM_{10} anomalies calculated over the period March 18–May 18, 2020. Following the same methodology, the absolute and relative differences between 2020 and the previous seven years are presented in a single figure, where the information on maps where each station is coloured depends on absolute differences and is sized based on the relative differences.

The NO_2 anomalies depict a clear reduction in mean concentrations (mostly $> 30\%$) during the lockdown all over Europe (Figure 1a). The strongest changes occur in Southern Europe (Spain, France, Italy) where the
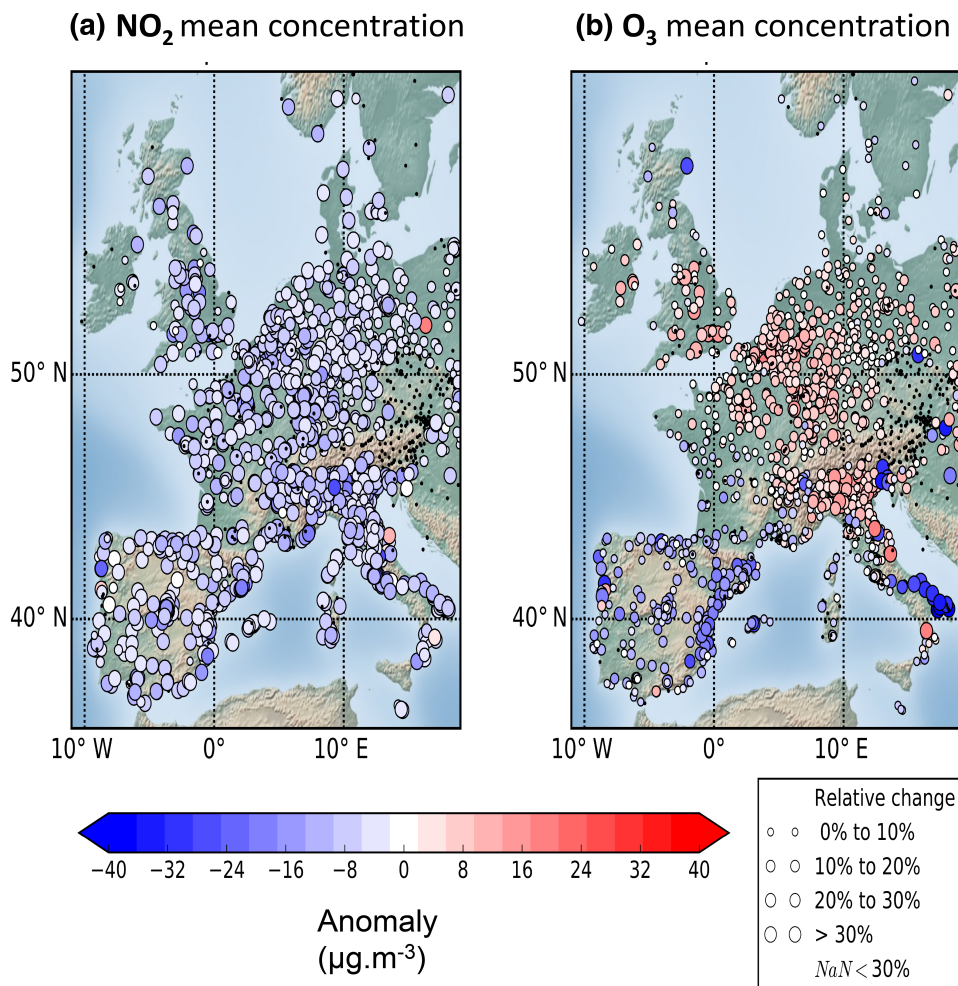

(a) NO$_2$ mean concentration **(b) O$_3$ mean concentration**

Relative change
- 0% to 10%
- 10% to 20%
- 20% to 30%
- > 30%
- NaN < 30%

Anomaly (µg.m^{-3})

FIGURE 1 Anomalies of (a) nitrogen dioxide (NO_2) mean concentration and (b) ozone (O_3) mean concentration at European Air Quality e-Reporting database (AirBase) stations in 2020 compared with the previous seven years (2013–2019) for the period March 18–May 18, 2020. Dots are coloured according to the anomalies in concentration (µg·m^{-3}) and sized proportionally to the relative change (%). Black dots correspond to stations with < 30% of available data

COVID-19 incidence has been among the highest (COVID-19.who.int), and where the strongest mobility restrictions were imposed. At two stations (see Figure S2 in Appendix S1 in the additional supporting information), the NO_2 concentrations are surprisingly greater in 2020 than during the seven previous years (anomaly > 10 μg·m^{-3}), which suggests recent increases in local emissions. Anomalies of the 50th percentile (median) and 90th percentile (P90) of daily maximum concentrations show the same spatial patterns (see Figure S3a and S3c in Appendix S1 in the additional supporting information).

Although the negative anomalies in NO_2 concentration occurred everywhere in Europe, regional patterns in O_3, with positive anomalies in the Benelux and negative anomalies in Spain, Portugal and southwestern France, can be clearly observed (Figure 1b). In the north of the continent, most of the stations reported positive anomalies in the mean concentrations (ranging from 0% to 30%), whereas in Southwestern Europe, negative anomalies were reported (ranging from 0% to −30%). In the region of the French and Italian Alps, the anomalies of O_3 were especially variable (> 30% and < −30%).

As for NO_2, anomalies in the 50th percentile (median) and 90th percentile (P90) of O_3 daily maximum concentrations are characterized by the same spatial patterns as the anomalies of the mean concentrations (see Figure S3b and S3d in Appendix S1 in the additional supporting information).

It was checked if the spatial patterns of PM_{10} anomalies could be related to the patterns of NO_2 and O_3. Negative PM_{10} anomalies in the mean and median of daily maximum concentrations in Northern and Southwestern Europe were found (see Figure S4 in Appendix S1 in the additional supporting information). In Italy and Benelux, there was no spatially consistent pattern in PM_{10} anomalies. Thus, PM_{10} anomalies do not match those of NO_2 and O_3.

The investigations are consistent with Ordóñez et al. (2020) in terms of spatial patterns and quantification of the O_3 anomalies, although they use a different methodology, reference period and definition of the lockdown duration. The contrast in O_3 anomalies between the North and Southwest of Europe does not correspond to the spatial patterns in the PM_{10} anomalies nor to the level of urbanization. Therefore, further analysis on the O_3 response is necessary, which is presented in the next section.

5 | O_3 RESPONSE ANALYSIS

A comprehensive analysis of the O_3 response to the emission reduction of air pollutants during the COVID-19 lockdown must consider the different potential drivers of O_3 changes. These include the emissions of precursor species such as NO_x, CO and volatile organic carbon (VOC), as well as surface dry deposition, together with the meteorological situation (atmospheric humidity and temperature, cloudiness and solar irradiance, precipitation, wind direction and speed, and intrusion of stratospheric air masses) (e.g. Monks et al., 2015). The analysis must also distinguish between regional (background) and local (urban) contributions.

The contribution of each process could not be quantified with the available data sets, but some evidence for the relative importance of their influence can be obtained. To document the spatial patterns of O_3 anomalies in Europe, the study analyses: (1) the transport of O_3 in Western Europe, (2) the meteorological disturbances, (3) the differences between urban and rural stations and (4) the relationship with NO_2 anomalies.

The study investigates modifications on the western border of the domain by examining observations at the "Mace head" station, a site representative of the baseline O_3 concentrations in the Northern Hemisphere at mid-latitude (Derwent et al., 2018). During the period under investigation, the O_3 concentration was in the range of the observations in the previous seven years (see Figure S5 in Appendix S1 in the additional supporting information). A modeling study supports the conclusion that the eastward transport of O_3 in the lowermost troposphere was slightly reduced during the study period (Gaubert et al., 2020). In addition, another study based on O_3 stations also reported a decrease of 7% from 1 to 8 km in altitude (Steinbrecht et al., 2020). The results and these studies indicate that the O_3 anomalies in Europe were not driven primarily by a change in background O_3, but rather by meteorological and emission changes.

During the lockdown period, the meteorology in Northern Europe, especially in the Benelux region, was characterized by anomalously low humidity (see Figure S6b and S6c in Appendix S1 in the additional supporting information), high pressure (see Figure S6d online), low cloudiness (Figure 2a), low wind speed (see Figures S6f, S6g and S6h online), high surface solar radiation (see Figure S6i online), and downward transport of air from the stratosphere (see Figure S6e online). These meteorological conditions are responsible for an enhancement in the O_3 concentration due to the increase in surface solar radiation and low humidity in the planetary boundary layer (Yu, 2019). A positive anomaly in the 2 m temperature was observed in France, south of the dry anomaly region (see Figure S6a online). In Southern Europe, specifically Spain, where O_3 concentrations were anomalously low, total cloud cover and relative humidity were particularly high and associated with low solar
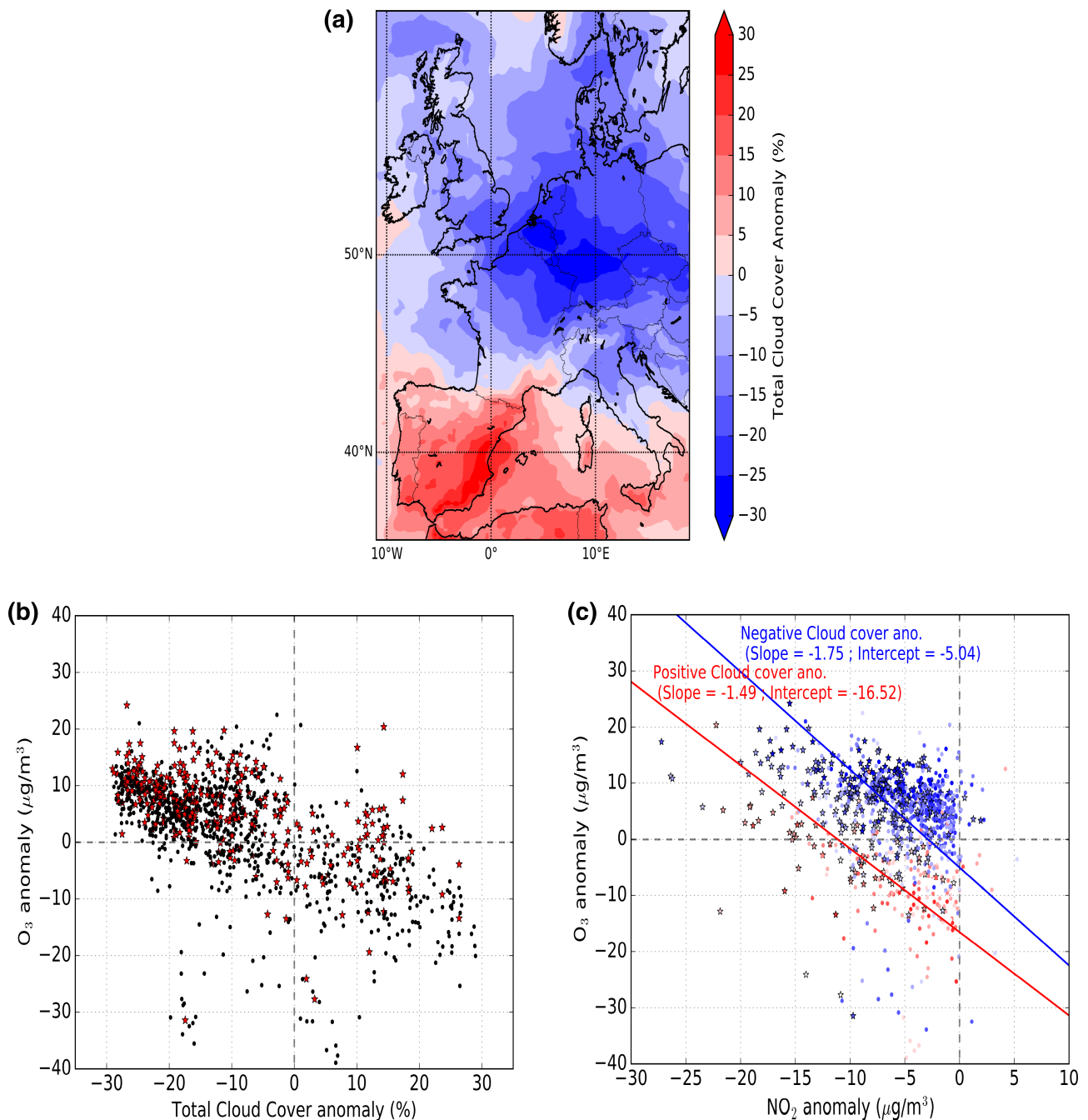
FIGURE 2 (a) Total cloud cover anomalies from the Copernicus Atmosphere Monitoring Service (CAMS) global forecast. Anomalies of the means in 2020 compared with the previous seven years (2013–2019) for the period March 18–May 18, 2020. (b) Ozone (O_3) anomalies against total cloud cover anomalies at European Air Quality e-Reporting database (AirBase) stations. (c) O_3 anomalies against nitrogen dioxide (NO_2) anomalies at AirBase stations. Stars in (b, c) represent "urban" stations; dots represent "rural" stations. "Urban" stations are defined by a population density threshold of 1,500 inhabitants·km^{-2}. Dots and stars in (c) are coloured depending on total cloud cover anomalies of (a) at each station. Blue and red lines are obtained by reduced major-axis regression restricted to positive and negative anomalies, respectively

radiation and temperature compared with the previous seven years.

The spatial patterns of several meteorological anomalies seem to match the O_3 anomalies. The study analyses, therefore, the correlation co-efficients of the anomalies in

the O_3 concentrations against the anomalies of 10 meteorological variables at each site (i.e. the corresponding grid cell). Correlation co-efficients were calculated for all monitoring stations, as well as for urban and rural stations separately (Table 2).

TABLE 2 Correlation co-efficients (R) between ozone (O_3) mean concentration anomalies and anomalies in (1) 2 m temperature, (2) 2 m dew point, (3) 2 m relative humidity, (4) mean sea level pressure, (5) potential vorticity at 300 hPa, (6) 10 m zonal wind speed, (7) 10 m meridional wind speed, (8) 10 m wind speed, (9) total cloud cover and (10) downward surface solar radiation

	Mean O_3 anomalies		
R	All	Urban	Rural
2 m-T ano.	0.20	0.14	0.18
2 m-Dew point ano.	−0.42	−0.46	−0.43
2 m-RH ano.	**−0.54**	**−0.56**	**−0.54**
Pot. Vort. 300 hPa ano.	0.43	0.47	0.44
MSL press. ano.	−0.35	−0.37	−0.33
10 m-Zonal wind ano.	−0.15	−0.19	−0.09
10 m-Merid. Wind ano.	−0.33	−0.42	−0.28
10 m-Wind speed ano.	0.25	0.24	0.26
Tot. cloud cov. ano.	**−0.61**	**−0.58**	**−0.61**
Surf. solar rad. down. ano.	**0.59**	**0.58**	**0.60**

Note: Anomalies are calculated for 2020 compared with the previous seven years (2013–2019) for the period March 18–May 18, 2020. The distinction between "urban" and "rural" sites is defined by a population density threshold of 1,500 inhabitants km^{-2}. Shown in bold font are $R > 0.5$ or $< −0.5$.

The signs of these correlation co-efficients (i.e. R) are consistent with the interpretation that specific meteorological conditions (less clouds, higher radiation, lower humidity, higher pressure) lead to an increase in the O_3 concentration. The spatial variability of the O_3 anomalies explained with meteorological variable anomalies (i.e. R^2) are highest for the total cloud cover ($R^2 = 0.36$), downward surface solar radiation ($R^2 = 0.35$) and 2 m relative humidity ($R^2 = 0.30$). Thus, the spatial variability of these meteorological anomalies is highly related with the spatial variability of O_3 anomalies (i.e. $R^2 = 0.30–0.36$).

The correlation co-efficients between the O_3 anomalies against meteorological anomalies are similar for urban and rural sites (Table 2), which suggests that the anomalies in the O_3 concentration are linked to the anomalies in the cloudiness (or radiation) across Europe during the lockdown period. Figure 2b shows that the O_3 anomalies follow the same linear relationship with the total cloud cover anomalies for urban as for other environments, which supports the interpretation of a regional scale influence of cloud cover (and therefore solar radiation) on O_3 anomalies.

The study accounts for the cloudiness in the O_3 against NO_2 scatterplot by colouring the dots as a function of the anomalies in the total cloud cover (Figure 2c). The total cloud cover anomalies add another layer of variability on top of this relationship because the

distribution of the blue and red dots in the scatterplot seems to follow two parallel lines. A reduced major axis regression is used in order to find the slope and intercept of the line that best summarizes the scatter plot of the O_3 anomalies against the NO_2 anomalies (Ayers, 2001). The slope obtained restricted to negative total cloud cover anomalies (−1.75) is lower than the slope obtained restricted to positive anomalies (−1.49). This result means that, for the same decrease in NO_2 concentration, the increase in O_3 concentration is stronger where the cloud cover was reduced (thus, solar radiation was increased). Moreover, the intercept is lower for positive anomalies (−16.52) than for negative cloud cover anomalies (−5.04), which suggests that the concentration of O_3 was higher where the cloud cover was reduced. This analysis of the two regression lines shows that the main processes leading to the spatial patterns of the O_3 anomalies (Figure 2a), involved solar radiation anomalies.

Radiation and cloudiness have played a major role in O_3's response to emission reductions. In addition, but to a lesser extent, the advection and subsidence of air masses (with a different level of O_3 concentration) could have contributed. Since the correlations between all meteorological variables are high, and nonlinear effects on O_3 are expected, it can only be concluded that cloud cover (and radiation) anomalies have largely contributed to the north-southwest contrast observed in the O_3 concentration anomalies in Europe during the COVID-19 lockdown.

6 | LEVEL OF TOTAL OXIDANT

In order to understand the specificity of the O_3 response during the lockdown, the spatial and temporal variability of daily mean total oxidant concentrations (i.e. $O_x \approx O_3 + NO_2$) is investigated. The study first investigates the spatial patterns of O_x anomalies at the regional scale (Section 6.1), and then focuses on urban environments, analysing the anomalies in day-to-day variability and in averaged diurnal cycles of NO_2, O_3 and O_x concentrations (Section 6.2).

6.1 | At the regional scale

Many processes can be invoked to explain the anomalies in surface total oxidant concentrations: (1) transport and deposition, (2) local photochemical production (thus related to the primary emissions of nitrogen and organic carbon), and (3) loss by oxidation of other atmospheric species (Jacob, 1999). However, a modification in the partitioning between O_3 and NO_2
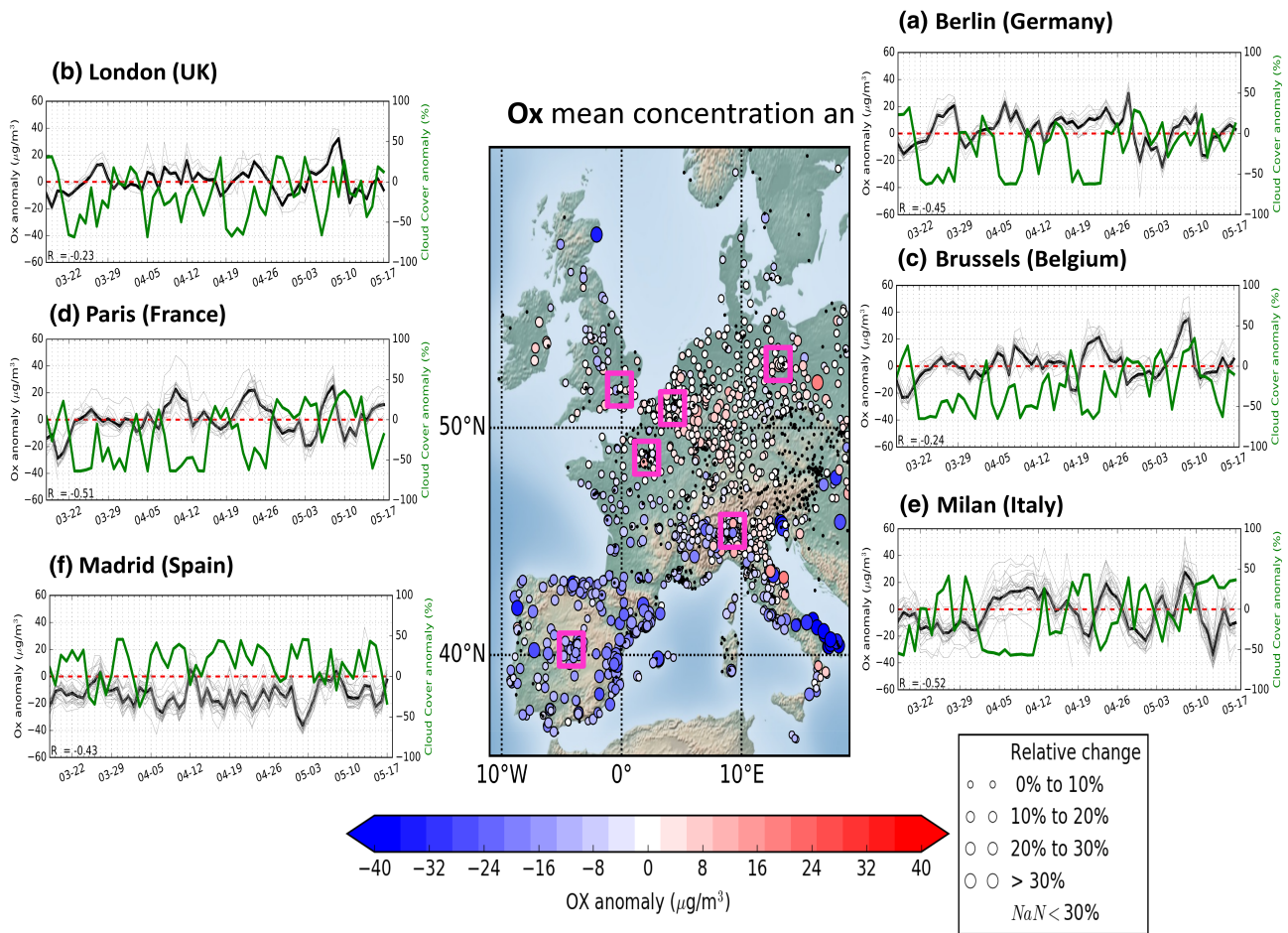
FIGURE 3 Map of mean total oxidant (O_x) concentration anomalies at European Air Quality e-Reporting database (AirBase) stations in 2020 compared with the previous seven years (2013–2019) for the period March 18–May 18, 2020. Dots are coloured according to the anomalies in concentration ($\mu g \cdot m^{-3}$) and sized proportionally to the relative change (%). Black dots correspond to stations with < 30% of available data. Violet squares correspond to the location of the six major European cities for which are presented the daily total clover cloud anomalies (green line) and daily O_x mean concentration anomalies compared with the average of the previous seven years at each station (grey lines) and for the average of all stations (black line) in (a) Berlin (Germany), (b) London (UK), (c) Brussels (Belgium), (d) Paris (France), (e) Milan (Italy) and (f) Madrid (Spain)

does not modify the level of total oxidant. The increase in O_3 concentrations coinciding with a NO_2 decrease is a consequence of the daytime photo-stationary state of O_3 (Leighton, 1961) in which the reaction of O_3 with NO (producing NO_2) is compensated by the photolysis of NO_2 (producing O_3).

Figure 3 presents a map of the mean O_x concentration anomalies in Europe compared with the previous seven years. In rural areas of Northern Europe (where $NO_2 \ll O_3$), the O_x anomalies are generally positive but low (< 20%). The situation is different in Southern Europe. In Southwestern Europe, the O_x anomalies are strongly negative, reaching −30% at several stations. In Italy, they are more variable with values ranging from −20% to 20%. In all urban areas (where $NO_2 \approx O_3$), the anomalies seem to be of the same order of magnitude as in the surrounding rural areas.

6.2 | In urban environments

Six major cities located in contrasted regions of the O_3 anomaly pattern are selected (Figure 1): Berlin (Germany), London (UK), Brussels (Belgium), Paris (France), Milan (Italy) and Madrid (Spain). Data were collected from all monitoring stations within $\pm 0.5°$ of the centre of these cities (that are defined as 13.4° E/52.5° N, 0.1° W/51.5° N, 4.3° E/50.8° N, 2.3° E/48.9° N, 9.2° E/45.4° N, 3.7° W/40.4° N, respectively).

Day-to-day variability and diurnal cycle anomalies are calculated for NO_2, O_3 and O_x concentrations as differences with the average of the previous seven years (Figures 3 and 4 and see Figure S7 in Appendix A in the additional supporting information). Anomalies are analysed based on 13 stations in Berlin, eight in London, 26 in Brussels, 31 in Paris, 28 in Milan and 27 in Madrid.
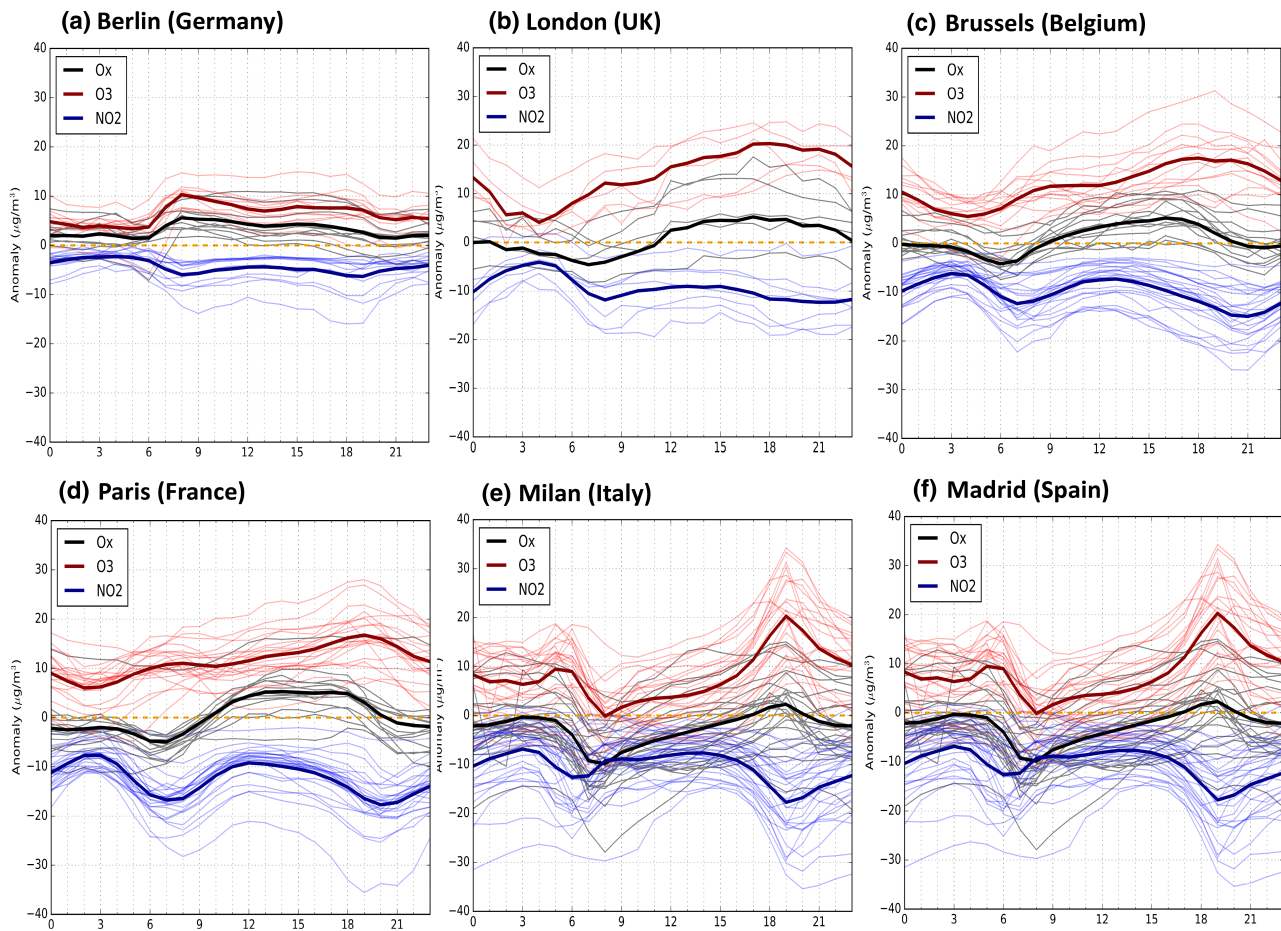
FIGURE 4 Hourly mean concentration anomalies of nitrogen dioxide (NO_2) (blue lines) and ozone (O_3) (red lines) in 2020 compared with the previous seven years (2013–2019) for the period March 18–May 18, 2020, for each monitoring station and for the average of all stations (bold lines) at six major European cities: (a) Berlin (Germany), (b) London (UK), (c) Brussels (Belgium), (d) Paris (France), (e) Milan (Italy) and (f) Madrid (Spain)

In each city, the variability between the individual stations is coherent, so that in the following, the focus is on the city average concentrations (Figures 3 and 4 and see Figure S7 online).

When examining the temporal variability of O_x in the six cities under consideration (Figure 3), the anomalies compared with previous years are small (typically ranging from −20 to 10 μg·m^{-3}). Madrid represents an exception with larger negative anomalies (ranging from −30 to 0 μg·m^{-3}). The periods of negative cloud cover anomaly match well the periods of positive O_3 anomaly. The daily total cloud cover anomalies are negatively correlated with the O_x anomalies, with the correlation co-efficients ranging from −0.23 to −0.52.

In the major cities of Northern Europe (i.e. Berlin, London, Brussels and Paris), NO_2 concentrations decreased and O_3 increased during the COVID-19 lockdown period (see Figure S7 in Appendix S1 in the additional supporting information). The NO_2 decrease was higher in Paris and Brussels, where lockdown restrictions

were stricter than in London and Berlin. In London, the lockdown effect on NO_2 concentrations was clearly visible after mid-April. In Milan, the NO_2 reduction was associated with a high day-to-day variability of the O_3 concentration during the entire period. Compared with the five other cities, Madrid is remarkable because for both NO_2 and O_3 the anomalies are negative.

Several relatively long periods of more than five consecutive days with negative cloud cover anomalies were observed in all cities, except Madrid. During these periods, O_x concentrations remained relatively constant and the observed increase in O_3 concentration was compensated by the decrease in NO_2 concentration. However, the correlation co-efficients between the anomalies in cloud cover and O_x concentration are variable in the six cities, ranging from −0.06 to −0.42. This is due to the occurrence of some specific events for which large increases in O_x reaching 20 μg·m^{-3} were observed during one or two days. Only half of these events were associated with negative cloud anomalies. Other processes

must therefore be invoked such as the transport of polluted air masses.

The study of the anomalies in the diurnal cycles of NO_2, O_3 and O_x concentrations provides useful information to confirm the authors' interpretation of the evolution of the level of total oxidant (Figure 4). Note that NO_2 anomalies remained negative throughout the day and night in all six cities. Except in Madrid, the O_3 anomalies remained positive throughout the day. In Berlin, total oxidant anomalies were positive throughout the day and night, ranging between 1 and 5 $\mu g \cdot m^{-3}$. In London, Brussels and Paris, the total oxidant level decreased overnight (about -5 $\mu g \cdot m^{-3}$) and increased during the day (about 5 $\mu g \cdot m^{-3}$) compared with the average observed over the previous seven years. In Milan, anomalies were (mostly) negative throughout the day and night, ranging between -10 and 1 $\mu g \cdot m^{-3}$. In Madrid, during the day and at night the level of total oxidant clearly decreased by > 10 $\mu g \cdot m^{-3}$.

In conclusion, the concentration of total oxidant decreased during the pandemics in Southwestern Europe, but remained similar to previous (unperturbed) years in Northern Europe. It appears that the observed O_3 increase in Northern Europe was due primarily to a change in the partitioning between O_3 and NO_2 as driven by positive solar radiation anomalies associated with reduced cloud cover. In addition, several episodes of positive O_x anomalies were noted during a few days, which could be linked to enhanced formation or reduced destruction of O_3, or to the transport of polluted air masses.

7 | SUMMARY AND PERSPECTIVES

The analysis confirms that the COVID-19 lockdown period in Europe has been exceptional in terms of (primary) pollutant concentration change, especially in the case of nitrogen dioxide (NO_2) whose concentration decrease was at least 14% for 90% of the monitoring stations relative to the previous seven years. The ozone (O_3) concentration response is contrasted between Northern and Southwestern Europe with positive and negative anomalies, respectively. Reduced cloud cover in Northern Europe coincided with the positive O_3 anomalies and was associated with a low increase of the level of total oxidant. Enhanced cloud cover in Southwestern Europe coincided with the negative O_3 anomalies associated with an important decrease of the level of total oxidant. Radiation and clouds played a major role in O_3's response to emission reductions. Air mass dynamics may have played a lesser role in the increase in O_3 (by advection or subsidence).

Episodes of high total oxidant level were observed in Northern Europe, but an assessment of the role of volatile organic carbons (VOCs) is necessary to quantitatively analyse changes in the chemical regime. Despite the lack of concordance of the anomalies of particulate matter (PM_{10}) and O_x, it cannot be excluded that aerosols have played an important role in O_3's response through the oxidation VOCs, through the production of inorganic aerosols, or through heterogeneous reactions affecting, for example, peroxy radicals (HO_2, RO_2), formaldehyde (HCHO), nitrogen oxides (NO) or O_3. Chemistry-transport models can provide these answers. Studies based on observations are essential to refine the estimates and to validate model outputs.

The results confirm the significant increase in surface concentrations of O_3 observed in most parts of Europe during the lockdown period and reported by Venter et al. (2020) and Ordóñez et al. (2020). Ordóñez et al. attributed this increase primarily to the influence of meteorological parameters rather than to the reduction in the emissions of primary pollutants. The present study concludes that the observed increase in O_3 was due primarily to a change in the photochemical partitioning between NO_2 and O_3 due to an anomalously low cloud cover, while the level of total oxidant remained unchanged, except in the Iberian Peninsula and southwestern France, where it decreased.

Understanding the behaviour of O_3 during the COVID-19 lockdown provides an opportunity to design future pollutant reduction regulations with the purpose of reaching the levels of NO_2 observed during the lockdown. Nevertheless, the study illustrates the complexity of the processes affecting O_3 in the troposphere and, hence, the difficulty of implementing efficient regulations targeting air quality impacts.

ORCID

Adrien Deroubaix https://orcid.org/0000-0003-4464-7802

Guy Brasseur https://orcid.org/0000-0001-6794-9497

Benjamin Gaubert https://orcid.org/0000-0002-6595-0686

Inga Labuhn https://orcid.org/0000-0003-3755-5264

Laurent Menut https://orcid.org/0000-0001-9776-0812

Guillaume Siour https://orcid.org/0000-0002-5940-4902

Paolo Tuccella https://orcid.org/0000-0003-0951-8773

REFERENCES

Air Quality e-Reporting (AQ e-Reporting) (2020). Available at https://www.eea.europa.eu/data-and-maps/data/aqereporting-8. Permanent link: b21a537e763e4ad9ac8ccffe987d6f77 [Accessed 22 July 2020].

Ayers, G.P. (2001) Comment on regression analysis of air quality data. *Atmospheric Environment*, 35(13), 2423–2425. https://doi.org/10.1016/S1352-2310(00)00527-6.

Bauwens, M., Compernolle, S., Stavrakou, T., Müller, J.-F., Gent, J., Eskes, H., Levelt, P.F., van der A.R., Veefkind, J.P., Vlietinck, J., Yu, H. and Zehner, C. (2020) Impact of coronavirus outbreak on NO 2 Pollution Assessed Using TROPOMI and OMI Observations. *Geophysical Research Letters*, 47(11), http://dx.doi.org/10.1029/2020gl087978.

CIESIN/CIAT. (2005) *Gridded Population of the World, Version 3 (GPWv3): Population Count Grid, Future Estimates*. Palisades, NY: NASA Socioeconomic Data and Applications Center (SEDAC). https://doi.org/10.7927/H42B8VZZ.Center for International Earth Science Information Network—CIESIN—Columbia University, United Nations Food and Agriculture Programme—FAO, and Centro Internacional de Agricultura Tropical—CIAT

Colette, A., Andersson, C., Baklanov, A., Bessagnet, B., Brandt, J., Christensen, J.H., Doherty, R., Engardt, M., Geels, C., Giannakopoulos, C., Hedegaard, G.B., Katragkou, E., Langner, J., Lei, H., Manders, A., Melas, D., Meleux, F., Rouïl, L., Sofiev, M., Soares, J., Stevenson, D.S., Tombrou-Tzella, M., Varotsos, K.V. and Young, P. (2015) Is the ozone climate penalty robust in Europe? *Environmental Research Letters*, 10(8), 084015. https://doi.org/10.1088/1748-9326/10/8/084015.

Derwent, R.G., Manning, A.J., Simmonds, P.G., Spain, T.G. and O'Doherty, S. (2018) Long-term trends in ozone in baseline and European regionally-polluted air at Mace head, Ireland over a 30-year period. *Atmospheric Environment*, 179(November 2017), 279–287. https://doi.org/10.1016/j.atmosenv.2018.02.024.

Doche, C., Dufour, G., Foret, G., Eremenko, M., Cuesta, J., Beekmann, M. and Kalabokas, P. (2014) Summertime tropospheric-ozone variability over the Mediterranean basin observed with IASI. *Atmospheric Chemistry and Physics*, 14(19), 10589–10600. https://doi.org/10.5194/acp-14-10589-2014.

Gaubert, B., Bouarar, I., Doumbia, T., Liu, Y., Stavrakou, T., Deroubaix, A.M., Darras, S., Elguindi, N., Granier, C., Lacey, F. G., Müller, J.-F., Shi, X., Tilmes, S., Wang, T. and Brasseur, G.P. (2020) Global changes in secondary atmospheric pollutants during the 2020 COVID-19 pandemic. *Pre-print*. https://doi.org/10.1002/essoar.10504703.1.

Goldberg, D.L., Anenberg, S.C., Griffin, D., McLinden, C.A., Lu, Z. and Streets, D.G. (2020) Disentangling the impact of the COVID-19 lockdowns on urban NO2 from natural variability. *Geophysical Research Letters*, 47(17), 0–3. https://doi.org/10.1029/2020GL089269.

Inness, A., Ades, M., Agustí-Panareda, A., Barré, J., Benedictow, A., Blechschmidt, A.-M., Dominguez, J.J., Engelen, R., Eskes, H., Flemming, J., Huijnen, V., Jones, L., Kipling, Z., Massart, S., Parrington, M., Peuch, V.-H., Razinger, M., Remy, S., Schulz, M. and Suttie, M. (2019) The CAMS reanalysis of atmospheric composition. *Atmospheric Chemistry and Physics*, 19(6), 3515–3556. https://doi.org/10.5194/acp-19-3515-2019.

Jacob, D.J. (1999) *Introduction to Atmospheric Chemistry*. Princeton, NJ: Princeton University press.

Kroll, J.H., Heald, C.L., Cappa, C.D., Farmer, D.K., Fry, J.L., Murphy, J.G. and Steiner, A.L. (2020) The complex chemical effects of COVID-19 shutdowns on air quality. *Nature Chemistry*, 12(9), 777–779. https://doi.org/10.1038/s41557-020-0535-z.

Le, T., Wang, Y., Liu, L., Yang, J., Yung, Y.L., Li, G. and Seinfeld, J. H. (2020) Unexpected air pollution with marked emission reductions during the COVID-19 outbreak in China. *Science*, 369, eabb7431. https://doi.org/10.1126/science.abb7431.

Leighton, P.A. (1961) *Reactions of Ozone, in Photochemistry of Air Pollution*, Vol. 9. New York: Elsevier, pp. 152–183.

Menut, L., Bessagnet, B., Siour, G., Mailler, S., Pennel, R. and Cholakian, A. (2020) Impact of lockdown measures to combat Covid-19 on air quality over western Europe. *Science of the Total Environment*, 741, 140426. https://doi.org/10.1016/j.scitotenv.2020.140426.

Monks, P.S., Archibald, A.T., Colette, A., Cooper, O., Coyle, M., Derwent, R., Fowler, D., Granier, C., Law, K.S., Mills, G.E., Stevenson, D.S., Tarasova, O., Thouret, V., von Schneidemesser, E., Sommariva, R., Wild, O. and Williams, M. L. (2015) Tropospheric ozone and its precursors from the urban to the global scale from air quality to short-lived climate forcer. *Atmospheric Chemistry and Physics*, 15(15), 8889–8973. https://doi.org/10.5194/acp-15-8889-2015.

Ordóñez, C., Garrido-Perez, J.M. and García-Herrera, R. (2020) Early spring near-surface ozone in Europe during the COVID-19 shutdown: meteorological effects outweigh emission changes. *Science of the Total Environment*, 747(December 2019), 141322. https://doi.org/10.1016/j.scitotenv.2020.141322.

Petetin, H., Bowdalo, D., Soret, A., Guevara, M., Jorba, O., Serradell, K. and Pérez García-Pando, C. (2020) Meteorology-normalized impact of the COVID-19 lockdown upon NO2 pollution in Spain. *Atmospheric Chemistry and Physics*, 20, 11119–11141. https://doi.org/10.5194/acp-20-11119-2020.

Shi, X. and Brasseur, G.P. (2020) The response in air quality to the reduction of Chinese economic activities during the COVID-19 outbreak. *Geophysical Research Letters*, 47(11), e2020GL088070. https://doi.org/10.1029/2020GL088070.

Sicard, P., De Marco, A., Agathokleous, E., Feng, Z., Xu, X., Paoletti, E., Rodriguez, J.J.D. and Calatayud, V. (2020) Amplified ozone pollution in cities during the COVID-19 lockdown. *Science of the Total Environment*, 735, 139542. https://doi.org/10.1016/j.scitotenv.2020.139542.

Steinbrecht, W., Kubistin, D., Plass-Dülmer, C., Davies, J., Tarasick, D.W., Gathen, P. von der., Deckelmann, H., Jepsen, N., Kivi, R., Lyall, N., Palm, M., Notholt, J., Kois, B., Oelsner, P., Allaart, M., Piters, A., Gill, M., Van Malderen, R., Delcloo, A.W., Sussmann, R., Mahieu, E., Servais, C., Romanens, G., Stübi, R., Ancellet, G., Godin-Beekmann, S., Yamanouchi, S., Strong, K., Johnson, B., Cullis, P., Petropavlovskikh, I., Hannigan, J.W., Hernandez, J-L, Diaz Rodriguez, A., Nakano, T., Chouza, F., Leblanc, T., Torres, C., Garcia, O., Röhling, A.N., Schneider, M., Blumenstock, T., Tully, M., Paton-Walsh, C., Jones, N., Querel, R., Strahan, S., Stauffer, R.M., Thompson, A.M., Inness, A., Engelen, R., Chang, K-L. and Cooper, OR. (2021) COVID-19 crisis reduces free tropospheric ozone across the northern hemisphere. *Geophysical Research Letters*, 48(5). http://dx.doi.org/10.1029/2020gl091987.

Venter, Z.S., Aunan, K., Chowdhury, S. and Lelieveld, J. (2020) COVID-19 lockdowns cause global air pollution declines. *Proceedings of the National Academy of Sciences*, 5(11), 202006853. https://doi.org/10.1073/pnas.2006853117.

Wang, Y. and Jacob, D.J. (1998) Anthropogenic forcing on tropospheric ozone and OH since preindustrial times. *Journal of Geophysical Research—Atmospheres*, 103(D23), 31123–31135. https://doi.org/10.1029/1998JD100004.

Wang, L., Li, M., Yu, S., Chen, X., Li, Z., Zhang, Y., Jiang, L., Xia, Y., Li, J., Liu, W., Li, P., Lichtfouse, E., Rosenfeld, D. and Seinfeld, J.H. (2020) Unexpected rise of ozone in urban and rural areas, and sulfur dioxide in rural areas during the coronavirus city lockdown in Hangzhou, China: implications for air quality. *Environmental Chemistry Letters*, 18(5), 1713–1723. https://doi.org/10.1007/s10311-020-01028-3.

Yan, Y., Lin, J., Pozzer, A., Kong, S. and Lelieveld, J. (2019) Trend reversal from high-to-low and from rural-to-urban ozone concentrations over Europe. *Atmospheric Environment*, 213 (January), 25–36. https://doi.org/10.1016/j.atmosenv.2019.05.067.

Yu, S. (2019) Fog geoengineering to abate local ozone pollution at ground level by enhancing air moisture. *Environmental Chemistry Letters*, 17(1), 565–580. https://doi.org/10.1007/s10311-018-0809-5.

SUPPORTING INFORMATION

Additional supporting information may be found online in the Supporting Information section at the end of this article.